

Acute stress induces long-term metabolic, functional, and structural remodeling of the heart

SUPPLEMENTARY INFORMATION

Supplementary Methods

2D Echocardiography

High resolution echocardiography was performed in B-mode and M-mode using a high-frequency ultrasound transducer (18 MHz, VEVO2100; Visualsonics). During the imaging sessions, rats were kept under isoflurane anesthesia with constant monitoring of heart and respiration rate and body temperature. Pulsed Doppler mode was used to measure transmitral blood flow velocities.

***In vivo* left coronary artery flow reserve measurements**

Coronary artery flow reserve (CFR) was measured with transthoracic US Doppler, using a high concentration of isoflurane (5% rate mixed in 100% air) as vasodilator (**CFR, extended data 2**). The pulsed Doppler probe was positioned over the proximal left anterior descending coronary artery and the coronary flow spectrum was characterized as a biphasic flow. The peak diastolic velocity at baseline (2% of isoflurane) and during hyperemia (5% of isoflurane over 5min) was measured, and the CFR was calculated as the ratio of the hyperemic to basal peak diastolic velocity.

Electrocardiogram (ECG)

ECG signals were recorded using 2 positive electrodes placed on the surface of the fore paws and 1 negative electrode placed on the surface of its left hind paw (PowerLab, ADInstruments, Sydney, Australia).

Noninvasive blood pressure measurement

Blood pressure was measured in the rat tail using the volume pressure recording sensor technology (tail-cuff CODA® High Throughput system, Kent Scientific).

Immunohistochemistry (IHC)

Each cardiac section was stained in triplicate for Periodic Acid Schiff (PAS) and oil-red. PAS and oil-red stainings were performed manually. Stained sections were scanned in their entirety with a NanoZoomer HT 2.0 (Hamamatsu) at a magnification of x20.

Second Harmonic Generation (SHG)

SHG and TPEF (Two-Photon Excitation Fluorescence) images were acquired with a nonlinear multiphoton Leica SP8 DIVE microscope (Leica microsystems GmbH, Wetzlar, Germany) coupled with a Coherent Discovery (Coherent Inc., Santa Clara, CA, USA) laser source. Three fields of view were acquired from paraffin embedded 4 µm-thick sections of apical and basal LV regions. To quantify SHG signal, the microscope settings were adjusted using a non-fibrotic control heart section. TPEF and SHG images were acquired with a 25x W 0.95 NA objective, excitation wavelength was 1040 nm at constant power and photomultiplier tubes and hybrid detectors were used at 800 V and 80% gain respectively. SHG score was proceeded using a homemade ImageJ macro from the IMAG'IC core facility.

Transmission electron microscopy

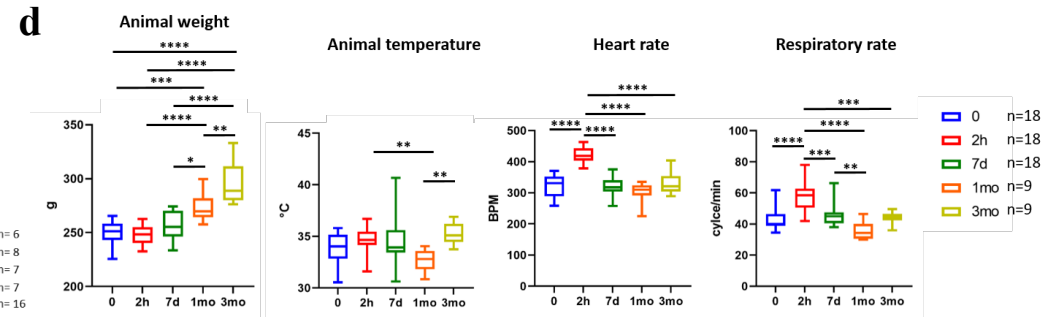
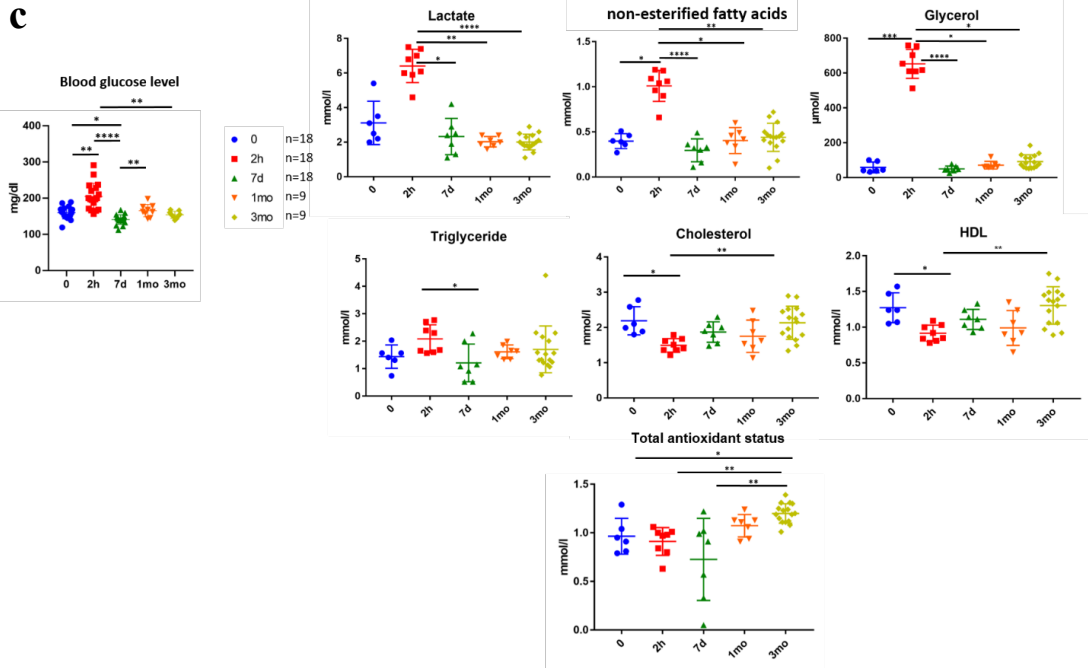
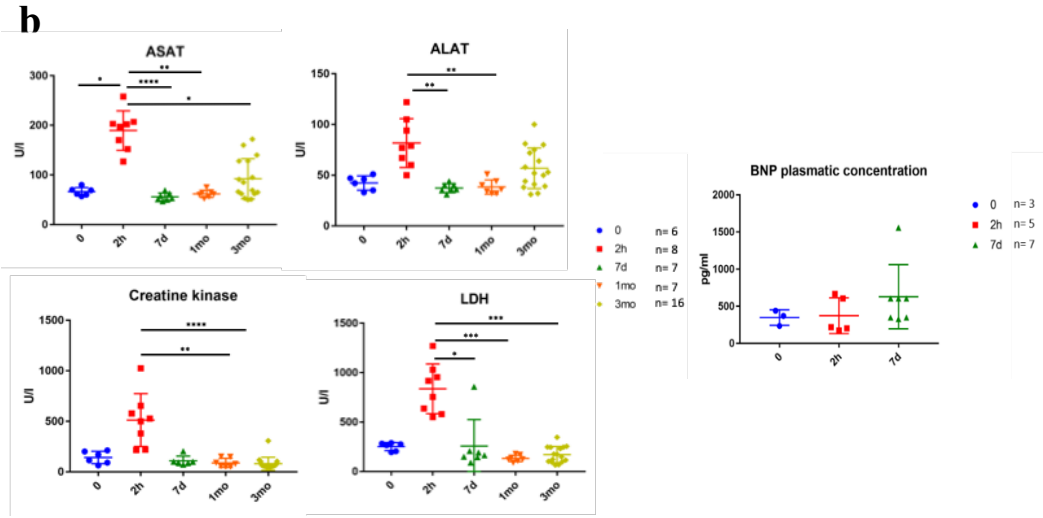
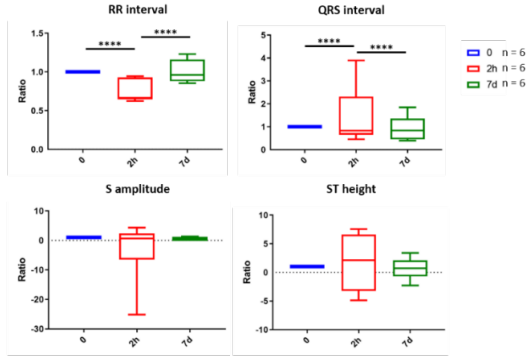
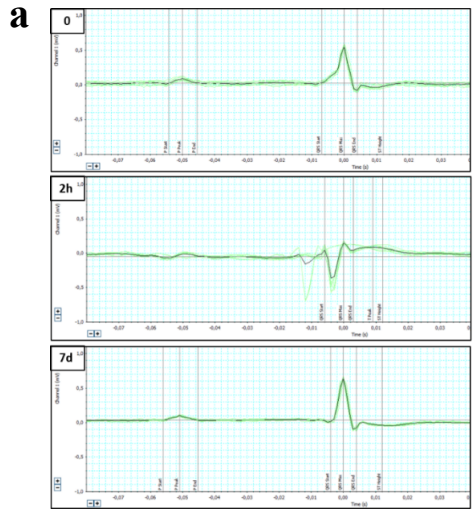
Apical and basal segments of the LV were fixed in Trump's fixative solution (#50 980 239, ThermoFisher), a combination of sodium cacodylate, formalin and glutaraldehyde, and dehydrated. Samples (1 cubic mm) were immersed twice in propylene oxide baths, in a prepolymer/propylene oxide mix, then left in a pure prepolymer, and finally embedded in gelatin capsules. Capsules were polymerized during at least 24 hours in an oven at 60°C. Samples were sectioned with a Reichert Ultracut S ultramicrotome. Semi-fine sections were taken to check the quality and orientation of the sample. They were then stained with toluidine blue and stored. Ultra-fine sections (90 nm thick) were cut with a diamond knife (Diatome). The ultrastructure images were observed with a transmission electron microscope JEOL 1011, (JEOL Ltd, Tokyo, Japan) using the camera GATAN Orius (AMETEK,

USA). Images were acquired with software Digital Micrograph® (AMETEK, USA) and exported in uncompressed tiff format.

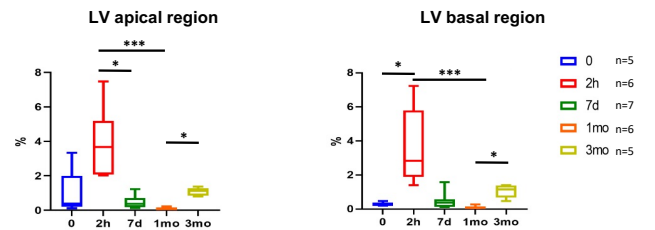
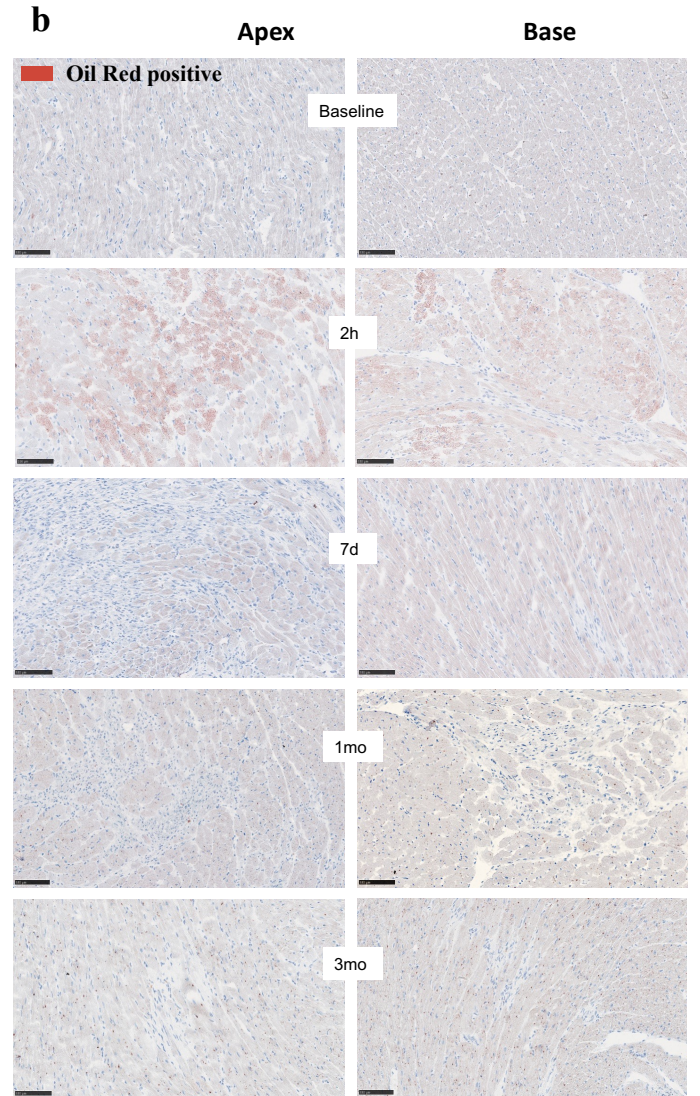
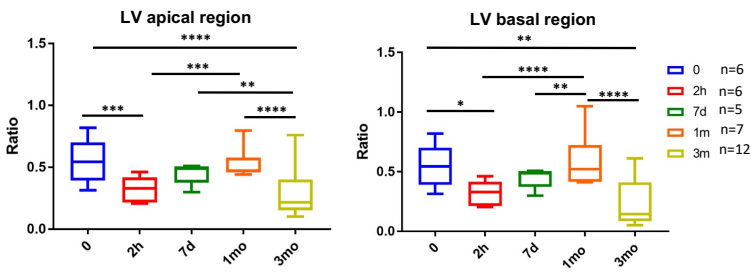
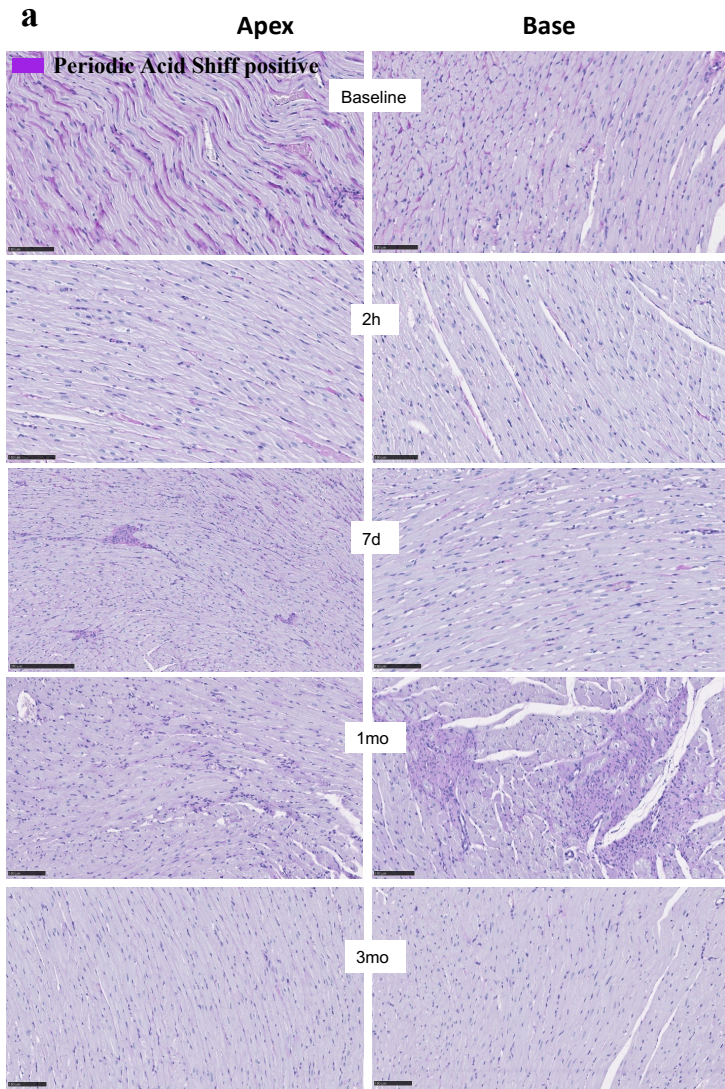
BNP plasmatic dosage

BNP plasmatic concentrations were measured by ELISA (RayBio Human/Mouse/Rat BNP enzyme Immunoassay kit, Norcross, Georgia, USA) according to the manufacturer's protocol. All samples were assayed in duplicate.

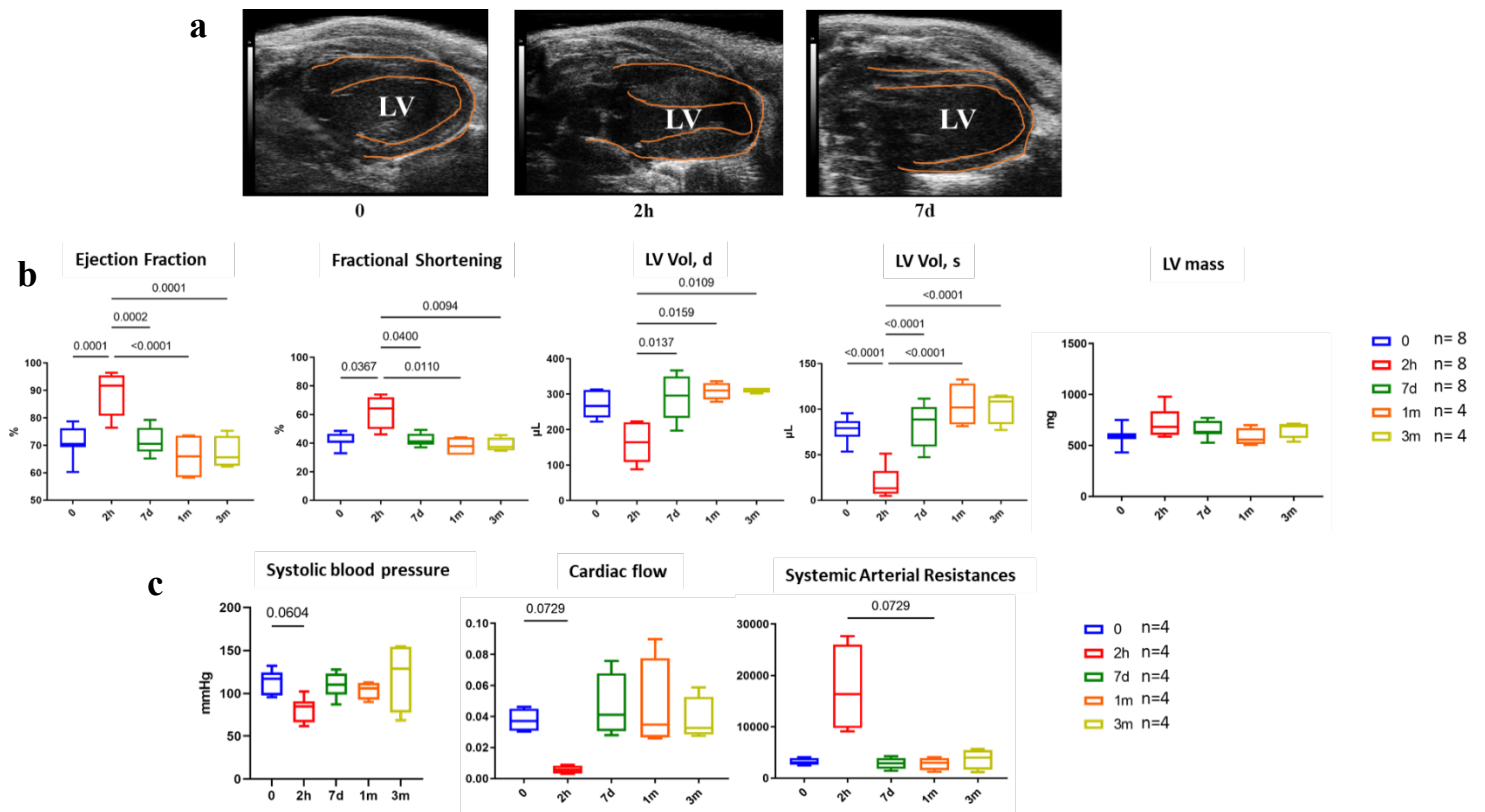
Supplementary figures



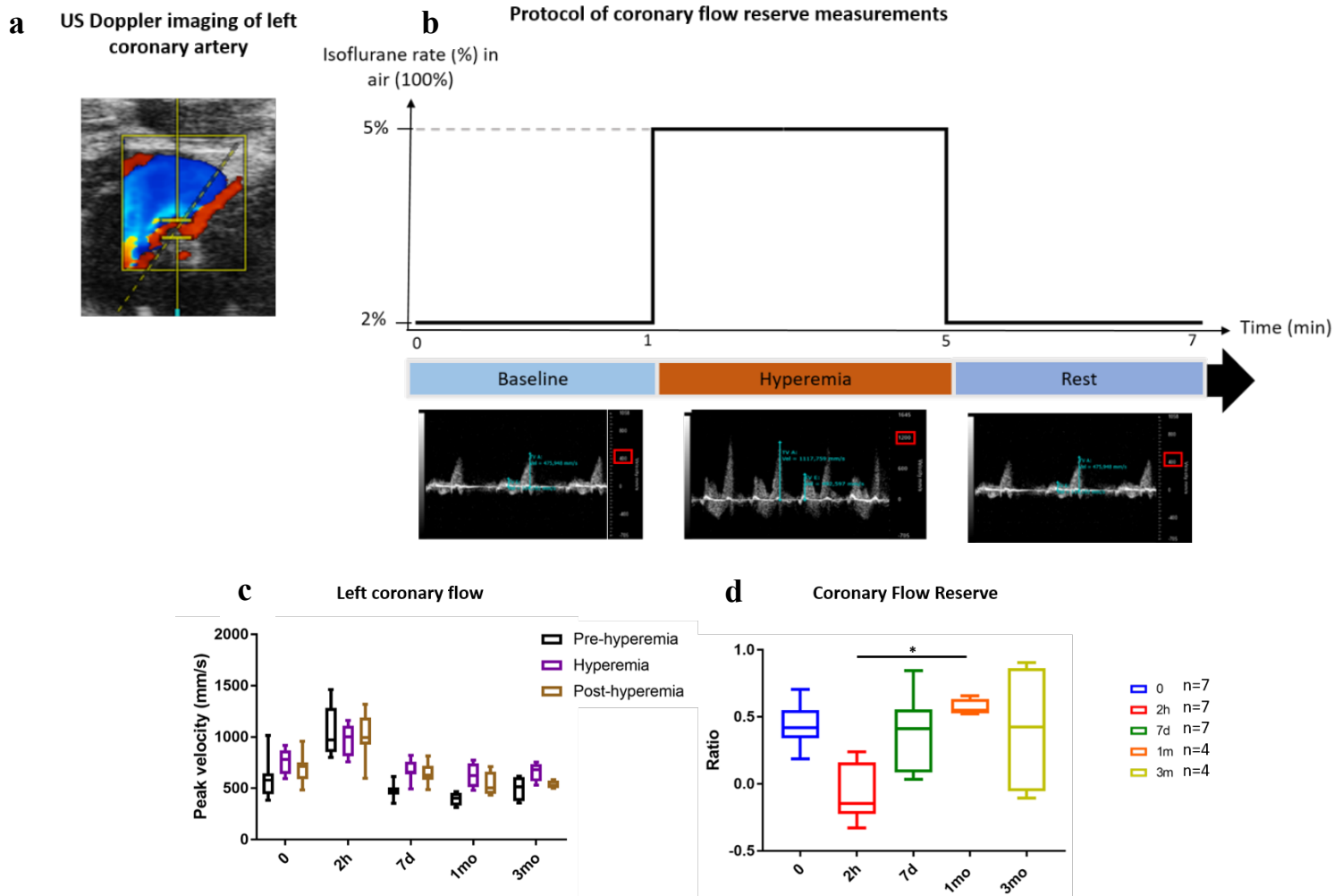
Supplementary figure 1. Effect of isoprenaline on electrocardiogram, plasmatic constants, and physiological constants. a Typical signs of acute stress were observed on the boxplots showing median, 25 and 75 percentiles, and extremes of electrocardiograms values of rats recorded 2h post intraperitoneal injection of isoprenaline (ISO, 50 mg/kg), notably a shortening of the RR interval (0 vs. 2h: $p < 0.0001$ and 2h vs. 7d: $p < 0.0001$) and a longer QRS interval (0 vs. 2h: $p < 0.0001$ and 2h vs. 7d: $p < 0.0001$). No statistically significant changes were found in the amplitude of the S wave or the height of the ST segment, although these parameters were highly variable during the acute-stress phase. **b** Plasmatic biomarkers of heart failure ASAT (0 vs. 2h: $p = 0.0377$, 2h vs. 7d: $p < 0.0001$, 2h vs. 1mo: $p = 0.0029$ and 2h vs. 3mo: $p = 0.0478$), ALAT (2h vs. 7d: $p = 0.0019$, and 2h vs. 1mo: $p = 0.0034$), Creatine kinase (2h vs. 1mo: $p = 0.0038$, and 2h vs. 3mo: $p < 0.0001$) and LDH (2h vs. 7d: $p = 0.0228$, 2h vs. 1mo: $p = 0.0003$, and 2h vs. 3mo: $p = 0.0003$) increased during the catecholaminergic surge and later returned to normal, while a modest increase of BNP was measured at 7d post stress. **c** The plasmatic concentrations of energy substrates glucose (0 vs. 2h: $p = 0.0076$, 0 vs. 7d: $p = 0.0274$, 2h vs. 7d: $p < 0.0001$, 2h vs. 3mo: $p = 0.0044$, and 7d vs. 1mo: $p = 0.0274$), lactate (2h vs. 7d: $p = 0.0160$, 2h vs. 1mo: $p = 0.0022$, and 2h vs. 3mo: $p < 0.0001$), non-esterified fatty acids (0 vs. 2h: $p = 0.0151$, 2h vs. 7d: $p < 0.0001$, 2h vs. 1mo: $p = 0.0173$, 2h vs. 3mo: $p = 0.0097$), glycerol (0 vs. 2h: $p = 0.0004$, 2h vs. 7d: $p < 0.0001$, 2h vs. 1mo: $p = 0.0164$, and 2h vs. 3mo: $p = 0.0290$), and triglyceride (2h vs. 7d: $p = 0.0209$) augmented at 2h post-ISO and then returned to normal. In contrast, cholesterol (0 vs. 2h: $p = 0.0200$, and 2h vs. 3mo: $p = 0.0080$) and HDL (0 vs. 2h: $p = 0.0482$, and 2h vs. 3mo: $p = 0.0043$) were lower at 2h and returned to pre-ISO values afterwards, while the total antioxidant status (0 vs. 3mo: $p = 0.0455$, 2h vs. 3mo: $p = 0.0026$, and 7d vs. 3mo: $p = 0.0031$) was unchanged except at the latest time point. **d** Boxplots showing median, 25 and 75 percentiles, and extremes of basic physiological parameters values: ISO increases heart rate (0 vs. 2h: $p < 0.0001$, 2h vs. 7d: $p < 0.0001$, 2h vs. 1mo: $p < 0.0001$, and 2h vs. 3mo: $p < 0.0001$) and respiratory rate (0 vs. 2h: $p < 0.0001$, 2h vs. 7d: $p = 0.0008$, 2h vs. 1mo: $p < 0.0001$, 2h vs. 3mo: $p = 0.0006$, and 7d vs. 1mo: $p = 0.0035$) during the acute phase only, body weight gain (0 vs. 1mo: $p = 0.0011$, 0 vs. 3mo: $p = 0.0002$, 2h vs. 1mo: $p = 0.0002$, 2h vs. 3mo: $p < 0.0001$, 7d vs. 1mo: $p = 0.0044$, 7d vs. 3mo: $p < 0.0001$, and 1mo vs. 3mo: $p = 0.0002$) and body temperature (2h vs. 1mo: $p = 0.0104$, and 1mo vs. 3mo: $p = 0.0011$) are unaffected by ISO. Unpaired comparison tests: * $p < 0.05$, ** $p < 0.01$ and *** $p < 0.001$. Statistical significance ($p < 0.05$) for each variable was estimated by one-way or two-way ANOVA when group variances were equal (Bartlett test); if not the non-parametric Kruskal-Wallis test, and the Holm multiple comparisons test was used to execute simultaneous t-tests. Source data are provided as a Source Data file.



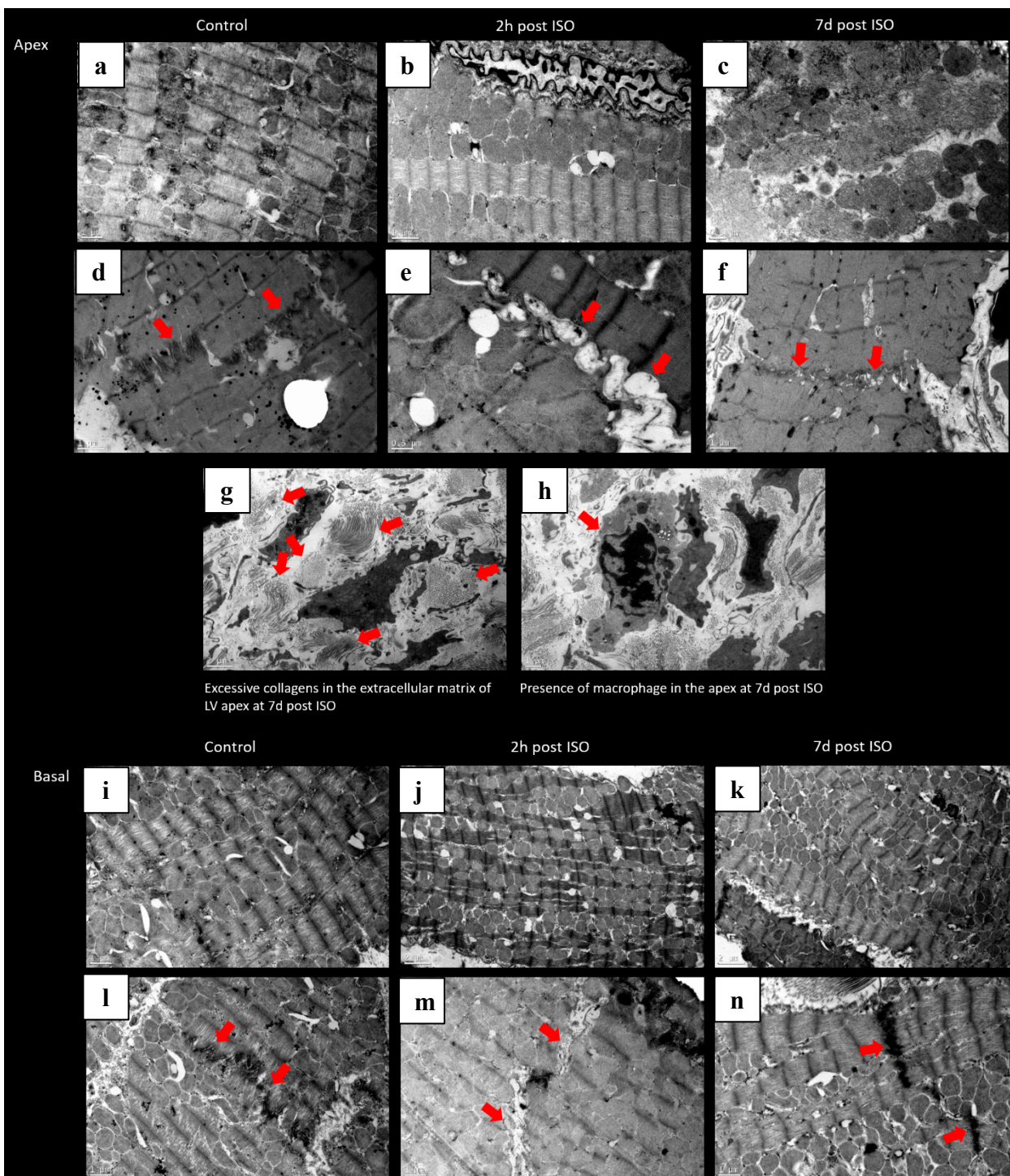
Supplementary figure 2. Cardiac reserves of energy substrates post-ISO. **a** Representative sections stained for glycogen by Periodic acid Schiff (PAS) at the indicated time points post-ISO represented in boxplots showing median, 25 and 75 percentiles, and extremes of values. Sections for the apex and base obtained from the same animal at each time point. Box plots for the indicated number of animals show a loss of glycogen deposits in the myocardium at 2h and at 3mo post-ISO both in the apex (0 vs. 2h: $p=0.0005$, 0 vs. 3mo: $p<0.0001$, 2h vs. 1mo: $p=0.0002$, 7d vs. 3mo: $p=0.0325$, and 1mo vs. 3mo: $p<0.0001$) and the base of the heart (0 vs. 2h: $p=0.0186$, 0 vs. 3mo: $p=0.0048$, 2h vs. 1mo: $p<0.0001$, 7d vs. 1mo: $p=0.0011$, and 1mo vs. 3mo: $p<0.0001$). **b** Representative sections stained for lipid droplets by Oil Red at the indicated time points post-ISO represented in boxplots showing median, 25 and 75 percentiles, and extremes of values. Sections for the apex and base obtained from the same animal at each time point. Box plots for the indicated number of animals show a transient increase of lipid droplets in the myocardium at 2h post-ISO both in the apex (0 vs. 2h: $p=0.1994$, 2h vs. 7d: $p=0.0379$, 2h vs. 1mo: $p=0.0001$, and 1mo vs. 3mo: $p=0.0436$) and the base (0 vs. 2h: $p=0.0482$, 2h vs. 1mo: $p<0.0001$, and 1mo vs. 3mo: $p=0.0385$) of the heart. Unpaired comparison tests: * $p<0.05$, ** $p<0.01$ and *** $p<0.001$. Statistical significance ($p<0.05$) for each variable was estimated by one-way or two-way ANOVA when group variances were equal (Bartlett test); if not the non-parametric Kruskal-Wallis test, and the Holm multiple comparisons test was used to execute simultaneous t-tests. Scale bars in the images correspond to a length of 100 μm . Source data are provided as a Source Data file.



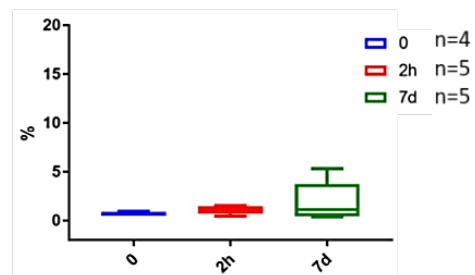
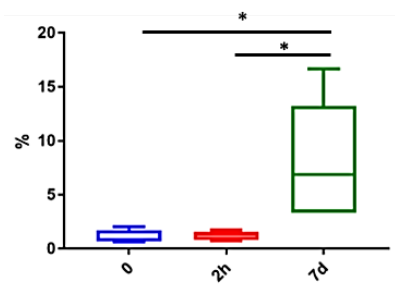
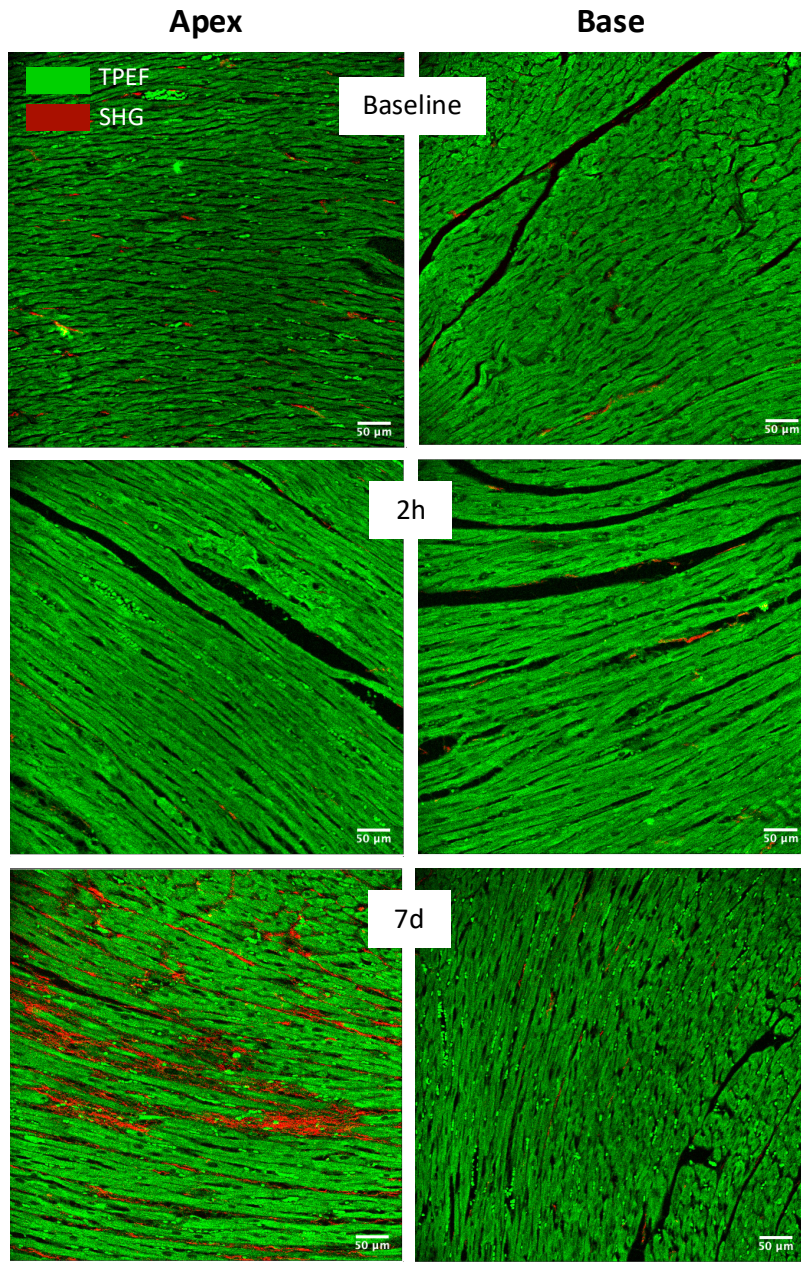
Supplementary figure 3. High resolution echocardiography. **a** Representative echocardiographic images of the LV of one animal showing a drastic reduction of the diastolic volume at 2h post ISO, followed by recovery at 7d post-ISO. **b** Boxplots showing median, 25 and 75 percentiles, and extremes of echocardiographic parameters at the indicated time points post-ISO. At 2h, the increase in the ejection fraction and fractional shortening are typical of the reduced LV volume during the diastolic (d) and systolic (s) phases. Both return later to normal. LV mass remains unchanged. **c** During the acute stress phase, systolic blood pressure and cardiac flow were reduced while systemic arterial resistances were increased, expected by the effect of ISO. Values represented in boxplots showing median, 25 and 75 percentiles, and extremes of values did not reach significance due to the small number of animals (n=4). All parameters recovered pre-ISO values by 7d post-ISO. Unpaired comparison tests. Statistical significance ($p < 0.05$) for each variable was estimated by one-way or two-way ANOVA when group variances were equal (Bartlett test); if not the non-parametric Kruskal-Wallis test, and the Holm multiple comparisons test was used to execute simultaneous t-tests. Source data are provided as a Source Data file.



Supplementary figure 4. Left coronary flow reserve measurements experiments. **a** Ultrasound Doppler imaging of a left coronary artery. **b** Protocol describing the induction of hyperemia using isoflurane. **c** LV coronary flow (CF, peak velocity in mm per second) in pre-hyperemic, hyperemic, and post-hyperemic conditions at baseline (n=8 animals) and 2h (n=8 animals), 7d (n=8 animals) and 1- (n=4 animals) and 3-months (n=4 animals) post-ISO, represented in boxplots showing median, 25 and 75 percentiles, and extremes of values. During the catecholaminergic surge, pre-hyperemic CF increases 1.7-fold. However, the CF is already maximal and not further increased by hyperemia. After the catecholaminergic surge, pre-hyperemic, hyperemic, and post-hyperemic CF return to pre-ISO values. **d** Time course of the coronary flow reserve ($CFR = (CF \text{ during hyperemia} - CF \text{ pre-hyperemia}) / CF \text{ pre-hyperemia}$) represented in boxplots showing median, 25 and 75 percentiles, and extremes of values depicting reduction at 2h post-ISO followed by recovery (2h vs. 1mo: $p=0.0495$). Unpaired comparison tests: * $p<0.05$, ** $p<0.01$ and *** $p<0.001$. Statistical significance ($p<0.05$) for each variable was estimated by one-way or two-way ANOVA when group variances were equal (Bartlett test); if not the non-parametric Kruskal-Wallis test, and the Holm multiple comparisons test was used to execute simultaneous t-tests. Source data are provided as a Source Data file.

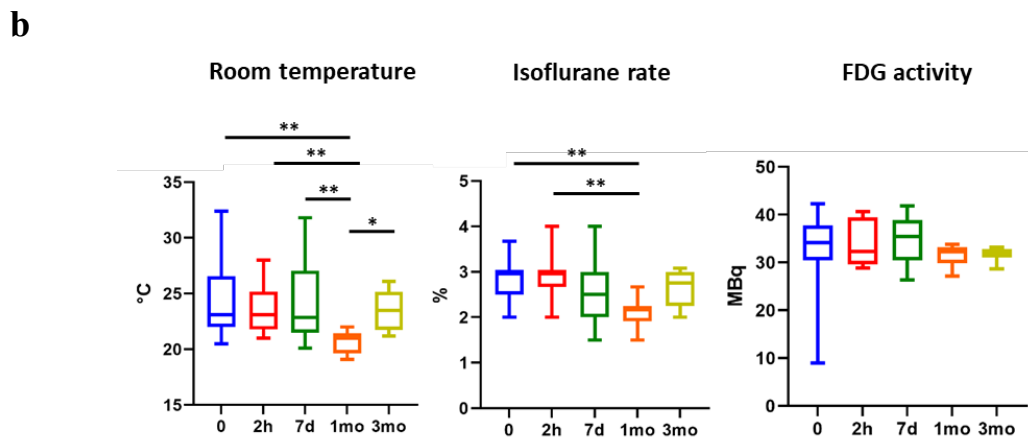
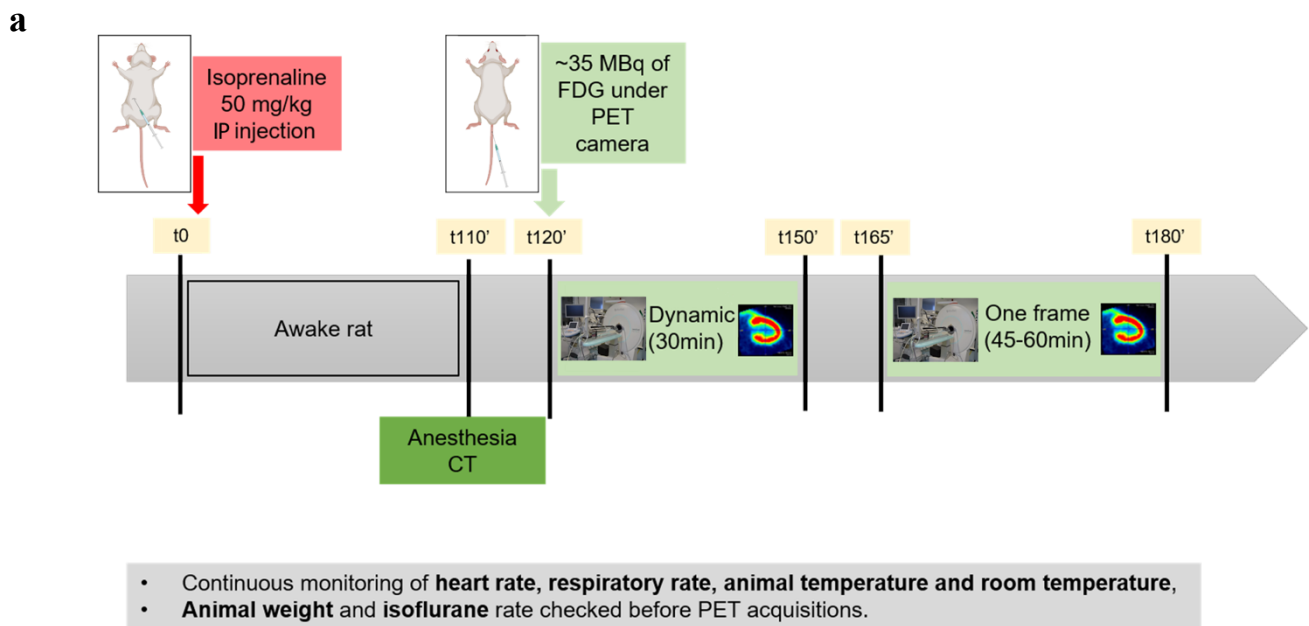


Supplementary figure 5. Transmission electron microscopy (TEM) of the heart ultrastructure at baseline, 2h, and 7 days post-ISO. Representative micrographs from n=5 hearts, in control (no-ISO), 2h and 7d post-ISO: **a-h** apical section, **i-k**: basal section of the heart. **a-c** Organization of the sarcomere fibers in the heart apex: normal orientation and alignment in the control group and at 2h post-ISO. **c** The normal alignment of cardiac myofibers was no longer recognizable in some fields of view at 7d post-ISO, while this was never observed pre-ISO or at 2h post-ISO. **d-f** The intercalated discs in the apex had a normal appearance in the control group but appeared disrupted at 2h post-ISO, suggesting a mechanical stress induced by ISO-induced hypercontractility. At 7d post-ISO intercalated discs were normal. **g** Important presence of collagens in the extracellular matrix at 7d post-ISO. **h** Every now and then, a phagocytic macrophage was observed at 7d post-ISO. No collagen deposits or macrophages were observed in the no-ISO control or the 2h post-ISO group. **i-k** Normal alignment and orientation of fibers in the basal region in the control group and at 2h and 7d post-ISO. **l-n** As in the apex, basal intercalated discs appeared transiently disrupted at 2h post-ISO and recovered their normal appearance afterwards. Scale bars in images **a, b, d, f, h, i, l, m** and **n** correspond to a length of 1 μm . Scale bars in images **c** and **e** correspond to a length of 0.5 μm . Scale bars in images **g, j** and **k** correspond to a length of 2 μm .



Supplementary figure 6. Second Harmonic Microscopy of cardiac tissue and SHG scores.

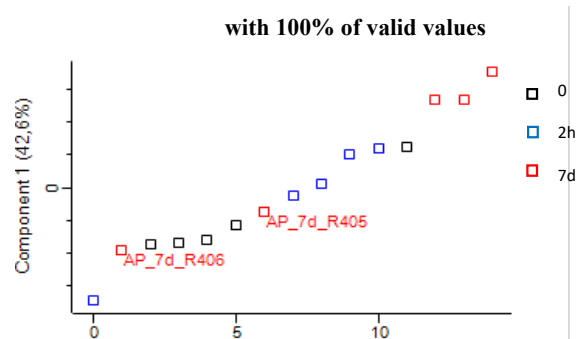
Representative fluorescence micrographs of n=3 fields-of-view per section from 8 sections (5 in the apex and 3 in the base) of n= 4 (baseline) and n=5 (2h and 7d post-ISO) hearts. TPEF: two-photon excited auto-fluorescence of the tissue, SHG: collagen-specific signal. Boxplots showing median, 25 and 75 percentiles, and extremes of values of the SHG score depicted a clear augmentation at 7d post-ISO in the apex (0 vs. 7d: $p=0.0173$, and 2h vs. 7d: $p=0.0467$), indicating a significant increase in cardiac collagen synthesis. Statistical significance ($p<0.05$) for each variable was estimated by one-way or two-way ANOVA when group variances were equal (Bartlett test); if not the non-parametric Kruskal-Wallis test, and the Holm multiple comparisons test was used to execute simultaneous t-tests. Scale bars in the images correspond to a length of 50 μm .



Supplementary figure 7. PET FDG acquisitions. **a** summarizes the protocol. PET FDG scans were acquired firstly dynamically for 30min after 30s post FDG i.v. injection, followed by 30min static acquisition. **b** Conditions of acquisitions were monitored systematically during the whole scans, such as room temperature (0 vs. 1mo: $p = 0.0014$, 2h vs. 1mo: $p = 0.0070$, 7d vs. 1mo: $p = 0.0072$, and 1mo vs. 3mo: $p = 0.0429$) and isoflurane rate (0 vs. 1mo: $p = 0.0084$ and 2h vs. 1mo: $p = 0.0014$), here represented in boxplots showing median, 25 and 75 percentiles, and extremes of values. No changes in injected FDG radioactivity were observed between the groups. Unpaired comparison tests: * $p < 0.05$, ** $p < 0.01$ and *** $p < 0.001$. $n = 18$ animals in groups from 0 to 7d post-ISO and $n = 9$ in groups 1mo and 3mo post-ISO.

a

Number of proteins identified by MS proteomics and of proteins used for group comparisons		
(L1)	Total number of identified proteins across all samples	4257
(L2)	Among (A), proteins with at least one LFQ	3203
(L3)	Among (B), proteins with at least 3 out of 5 LFQ in at least one group	2618
(L4)	Proteins with a LFQ in each sample	971

b 1D principal component analysis related to proteins**Supplementary figure 8. Proteomic analysis.**

a Number of proteins identified by MS proteomics used for group comparisons, indicating the levels (L) of stringency, $L1 < L2 < L3 < L4$. L1. Unfiltered data from the LFQ intensity columns of the *proteingroup.txt* file of MaxQuant output, corresponding to proteins identified with an intensity value in at least one sample, yet without necessarily a sufficient level of confidence and correlation across the proteins' distinct peptide intensities to qualify for quantification. L2: Proteins bearing at least one value in the LFQ intensity columns of the *proteingroup.txt* file of MaxQuant output. L3: Proteins filtered to show enough valid values for statistical analysis (3/5 samples in at least one group). These are the proteins listed in the table of Supplementary table 1. L4: Proteins with an LFQ value in every sample. **b** 1D representation of the component 1 of the principal component analysis (PCA) related to proteins with 100% of valid values (proteins that have LFQ intensity value for all conditions) in the LV apex. The two apical 7d post-ISO “outliers” (R405 and R406 in red) showed a lower performance in protein identifications with around 25% less identifications compared to all other samples and are located in the control side (in black) while the three apical samples (in red) of the five 7d post-ISO samples distinguished from the control and 2h post-ISO groups, indicating a clear post-ISO phenotype.

Canonical Pathways involved in apical metabolism remodeling	2h vs 0			7d vs 0		
	p-value	z-score	involved proteins	p-value	z-score	involved proteins
Insulin Secretion Signaling Pathway	1.04E-01	1.342	EIF4G2,PABPC1,PLCB3,RAP1B,SRP54	3.03E-01	2.828	ADCY6,CAMK2D,CAMK2G,EF4G2,EF4G3,MTOR,PABPC1,PLCB3
Insulin Receptor Signaling	4.20E-01	NaN	AKT2,RAP1B	1.60E-01	1.633	AKT2,GYS1,INPPL1,MTOR,PPP1CB,PPP1cc
PI3K/AKT Signaling	4.37E-02	0.000	AKT2,ELP1,PPP2R2A,RAP1B,THEM4	1.02E-02	1.000	AKT2,GYS1,INPPL1,ITGA6,MTOR,PPP2R3A,PPP2R5E,THEM4,YWHAE,YWHAQ,YWHAZ
14-3-3-mediated Signaling	1.39E-01	NaN	AKT2,PLCB3,RAP1B	1.13E-01	2.236	AKT2,PLCB3,TUBA1C,YWHAE,YWHAQ,YWHAZ
3-phosphoinositide Degradation	1.00E+00	NaN	PDXP	2.23E-01	2.236	ALPL,INPPL1,PALD1,PPP1cc,PPP2R3A,PPP2R5E
3-phosphoinositide Biosynthesis	1.00E+00	NaN	PDXP	4.39E-01	2.000	ALPL,PALD1,PPP1cc,PPP2R3A,PPP2R5E
D-myo-inositol-5-phosphate Metabolism	4.78E-01	NaN	PDXP,PLCB3	2.27E-01	2.236	ALPL,PALD1,PLCB3,PPP1cc,PPP2R3A,PPP2R5E
Superpathway of Inositol Phosphate Compounds	1.00E+00	NaN	PDXP,PLCB3	2.68E-01	2.449	ALPL,INPPL1,PALD1,PLCB3,PPP1cc,PPP2R3A,PPP2R5E
D-myo-inositol (3,4,5,6)-tetrakisphosphate Biosynthesis	1.00E+00	NaN	PDXP	3.08E-01	2.000	ALPL,PALD1,PPP1cc,PPP2R3A,PPP2R5E
D-myo-inositol (1,4,5,6)-Tetrakisphosphate Biosynthesis	1.00E+00	NaN	PDXP	3.08E-01	2.000	ALPL,PALD1,PPP1cc,PPP2R3A,PPP2R5E
AMPK Signaling	1.84E-01	NaN	AKT2,PPP2R2A,RAB3A,STIM1	2.82E-02	0.816	AK2,AKT2,GYS1,MTOR,PFKM,PFKP,PPM1E,PPP2R3A,PPP2R5E,PRKAB1,STIM1
Glycolysis I	—	—	—	4.47E-03	-1.000	GAPDH,PFKM,PFKP,PGAM2
Gluconeogenesis I	2.37E-01	NaN	ME3	4.47E-03	-1.000	GAPDH,MDH1,ME3,PGAM2
Oxidative Phosphorylation	3.80E-03	0.447	COX15,NDUFA3,NDUFB4,NDUFB6,NDUFB8	3.55E-07	-1.604	ATP5F1A,ATP5MC1,ATP5PO,ATPAF1,Cox7a2/Cox7a2l2,CYB5A,NDUFA6,NDUFA8,NDUFA9,NDUFB10,NDUFB4,NDUFB7,NDUFB8,NDUFS7
Fatty Acid β -oxidation I	—	—	—	1.10E-02	NaN	ECHDC3,ECHS1,HADHA,HADHB
Acetyl-CoA Biosynthesis III (from Citrate)	—	—	—	—	—	—
Acetyl-CoA Biosynthesis I (Pyruvate Dehydrogenase Complex)	6.31E-02	NaN	DBT	—	—	—

Symbol	Gene Name	2h vs 0		7d vs 0	
		p-value	Fold Change	p-value	Fold Change
FABP3	fatty acid binding protein 3	—	—	7.08E-03	-1.554
FABP4	fatty acid binding protein 4	—	—	1.63E-02	-1.373

Supplementary table 1. Analysis of canonical pathways involved in apical metabolism. Shown are significant changes in the canonical pathways as defined by Ingenuity Pathway Analysis software, based on mass spectrometry analysis of tissue extracts from n=5 animals for each time point. Comparative p values and z-scores between baseline (no-ISO) and 2h post-ISO animals, and baseline and 7d post-ISO, respectively. Significantly over-represented terms (canonical pathways, functions, upstream regulators) were identified with a right-tailed Fisher's Exact Test that calculates an overlap p-value. The z-score was also calculated to assess the activation (positive z-score) or repression (negative one) of each term. The mass spectrometry proteomics data have been deposited to the ProteomeXchange Consortium via the PRIDE partner repository with the dataset identifier [PXD032667](https://www.ebi.ac.uk/pride/archive/study/PXD032667).

Canonical Pathways involved in apical tissue remodeling	2h vs. 0		7d vs. 0	
	p-value	z-score	involved proteins	involved proteins
Cardiac β -adrenergic Signaling	1.00E+00	NaN	PPP2R2A	3.09E-02 -0.816
cAMP-mediated signaling	-	-	-	3.92E-01 2.449
mTOR Signaling	1.29E-06	1.000	AKT2,Cdc42,EIF3A,EIF3,EIF4G2,PPP2R2A,RAP1B,RHOT2,RPS11,RPS12,RPS16,RPS18	2.69E-05 1.134
p70S6K Signaling	1.15E-02	1.342	AKT2,F2,PLCB3,PPP2R2A,RAP1B	7.59E-03 1.342
Regulation of eIF4 and p70S6K Signaling	8.91E-07	NaN	AKT2,EIF3A,EIF3,EIF4G2,PABPC1,PPP2R2A,RAP1B,RPS11,RPS12,RPS16,RPS18	9.12E-05 NaN
Role of NFAT in Cardiac Hypertrophy	3.85E-01	NaN	AKT2,PLCB3,RAP1B	2.11E-01 2.121
Natural Killer Cell Signaling	1.06E-01	0.000	AKT2,COL18A1,HSPA1A/HSPA1B,RAP1B	3.11E-01 1.633
IL-6 Signaling	1.07E-02	-1.000	AKT2,CSNK2A1,ELP1,HSPB3,RAP1B	2.50E-01 0.447
IL-8 Signaling	1.70E-02	1.000	AKT2,Cdc42,ELP1,RAP1B,RHOT2,ROCK2	7.94E-02 2.121
Phospholipase C Signaling	2.52E-01	NaN	Cdc42,PLCB3,RAP1B,RHOT2	2.06E-01 0.447
HIF1 α Signaling	3.41E-01	NaN	AKT2,HSPA1A/HSPA1B,RAP1B	8.32E-02 1.414
Production of Nitric Oxide and Reactive Oxygen Species in Macrophages	2.88E-03	2.000	AKT2,APOA1,Cdc42,ELP1,PPP2R2A,RAP1B,RHOT2	1.10E-01 0.816
HIPPO signaling	2.09E-01	NaN	PPP2R2A,SKP1	3.09E-04 -2.000
Hepatic Fibrosis Signaling Pathway	1.93E-01	1.633	AKT2,Cdc42,COL18A1,RAP1B,RHOT2,ROCK2	1.00E+00 2.121
Regulation of Actin-based Motility by Rho	2.72E-01	NaN	Cdc42,RHOT2	1.20E-03 1.134
Integrin Signaling	1.78E-01	NaN	AKT2,Cdc42,RAP1B,RHOT2	5.13E-05 2.840
Actin Cytoskeleton Signaling	2.02E-01	1.000	F2,FN1,RAP1B,ROCK2	3.09E-04 1.291
Actin Nucleation by ARP-WASP Complex	8.32E-03	NaN	Cdc42,RAP1B,RHOT2,ROCK2	1.58E-02 2.000
Glutathione Redox Reactions I	2.20E-01	NaN	GSR	3.31E-03 -2.000
Glutathione-mediated Detoxification	2.69E-01	NaN	LANCL1	7.76E-03 -1.000
Apelin Cardiomyocyte Signaling Pathway	2.72E-01	NaN	AKT2,PLCB3	4.68E-02 0.816
Apelin Endothelial Signaling Pathway	1.20E-01	NaN	AKT2,PLCB3,RAP1B	8.91E-02 1.633
Xenobiotic Metabolism General Signaling Pathway	4.42E-01	NaN	AKT2,RAP1B	3.35E-01 -1.342
Xenobiotic Metabolism PXR Signaling Pathway	1.00E+00	NaN	ALDH16A1	8.51E-03 -1.508
Xenobiotic Metabolism CAR Signaling Pathway	5.55E-01	NaN	ALDH16A1,PPP2R2A	1.02E-01 -2.121
Xenobiotic Metabolism AHR Signaling Pathway	5.75E-01	NaN	ALDH16A1	2.14E-02 -2.449
Adrenomedullin signaling pathway	5.25E-02	0.447	AKT2,C3,CFH,PLCB3,RAP1B	1.00E+00 2.000
Estrogen Receptor Signaling	4.33E-01	0.000	AKT2,PLCB3,RAP1B,ROCK2	1.53E-01 1.155
GNRH Signaling	5.38E-01	NaN	PLCB3,RAP1B	1.77E-01 2.449

Supplementary Table 2. Analysis of canonical pathways involved in apical tissue remodeling.

Shown are significant changes in the canonical pathways implicated in apical tissue remodeling, as defined by Ingenuity Pathway Analysis software, based on mass spectrometry analysis of tissue extracts from n=5 animals for each time point. Comparative p values and z-scores between baseline (no-ISO) and 2h post-ISO animals, and baseline and 7d post-ISO, respectively. Significantly over-represented terms (canonical pathways, functions, upstream regulators) were identified with a right-tailed Fisher's Exact Test that calculates an overlap p-value. The z-score was also calculated to assess the activation (positive z-score) or repression (negative one) of each term. The mass spectrometry proteomics data have been deposited to the ProteomeXchange Consortium via the PRIDE partner repository with the dataset identifier [PXD032667](https://www.ebi.ac.uk/PRIDE/archive/PXD032667).

Canonical Pathways involved in apical vascular remodeling	2h vs. 0			7d vs. 0		
	p-value	z-score	involved proteins	p-value	z-score	involved proteins
VEGF Signaling	8.51E-02	NaN	AKT2,RAP1B,ROCK2	1.25E-01	1.000	ACTN1,ACTN2,ACTN4,AKT2,YWHAE
P2Y Purigenic Receptor Signaling Pathway	1.47E-01	NaN	AKT2,PLCB3,RAP1B	4.39E-01	1.000	ADCY6,AKT2,GNAI2,PLCB3
P2Y Purigenic Receptor Signaling Pathway	1.47E-01	NaN	AKT2,PLCB3,RAP1B	4.39E-01	1.000	ADCY6,AKT2,GNAI2,PLCB3
Coagulation System	1.51E-06	0.816	F2,FGA,FGG,PLG,SERPIND1,SERPINF2	2.40E-01	NaN	A2M,F13A1

Supplementary Table 3. Analysis of canonical pathways involved in apical vascular remodeling.

Shown are significant changes in the canonical pathways implicated apical vascular remodeling, as defined by Ingenuity Pathway Analysis software, based on mass spectrometry analysis of tissue extracts from n=5 animals for each time point. Comparative p values and z-scores between baseline (no-ISO) and 2h post-ISO animals, and baseline and 7d post-ISO, respectively. Significantly over-represented terms (canonical pathways, functions, upstream regulators) were identified with a right-tailed Fisher's Exact Test that calculates an overlap p-value. The z-score was also calculated to assess the activation (positive z-score) or repression (negative one) of each term. The mass spectrometry proteomics data have been deposited to the ProteomeXchange Consortium via the PRIDE partner repository with the dataset identifier [PXD032667](https://www.ebi.ac.uk/PRIDE/archive/PXD032667).

Canonical Pathways involved in basal metabolic remodeling	2h vs. 0			7d vs. 0		
	p-value	z-score	Involved proteins	p-value	z-score	Involved proteins
Insulin Receptor Signaling	4.57E-03	0.816	AKT2,GSK3A,INPPL1,MAP2K2,MAPK3,PPP1R7	1.86E-01	NaN	INPPL1,PPP1R7,SLC2A4,TRIP10,VAMP2
Insulin Secretion Signaling Pathway	1.31E-01	0.447	MAPK3,NSF,SRP54,SRP68,YES1	1.70E-02	1.508	CAMK2G,EIF2A,EIF2S2,EIF4G3,MAPK14,SLC2A4,SRP14,SSR1,STAT5B,VAMP2,YES1
Oxidative Phosphorylation	2.57E-02	1	ATP5PF,COX6A2,DMAC2L,NDUFB6	6.31E-03	0.378	ATP5PF,COX6B1,NDUFA5,NDUFAB1,NDUFB4,NDUFB8,NDUFS7

Supplementary Table 4. Analysis of canonical pathways involved in basal metabolic remodeling.

Shown are significant changes in the canonical pathways implicated in basal metabolic remodeling, as defined by Ingenuity Pathway Analysis software, based on mass spectrometry analysis of tissue extracts from n=5 animals for each time point. Comparative p values and z-scores between baseline (no-ISO) and 2h post-ISO animals, and baseline and 7d post-ISO, respectively. Significantly over-represented terms (canonical pathways, functions, upstream regulators) were identified with a right-tailed Fisher's Exact Test that calculates an overlap p-value. The z-score was also calculated to assess the activation (positive z-score) or repression (negative one) of each term. The mass spectrometry proteomics data have been deposited to the ProteomeXchange Consortium via the PRIDE partner repository with the dataset identifier [PXD032667](https://www.ebi.ac.uk/PRIDE/archive/PXD032667).

Canonical Pathways involved in basal vascular remodeling	2h vs. 0			7d vs. 0		
	p-value	z-score	Involved proteins	p-value	z-score	Involved proteins
P2Y Purigenic Receptor Signaling Pathway	1.45E-02	1	AKT2,GNAI3,GNB2,MAP2K2,MAPK3	#N/A	_	#N/A
Coagulation System	7.08E-03	NaN	F9,FGA,FGG	1.81E-01	NaN	A2M,F13A1
Thrombin Signaling	8.32E-02	2	AKT2,GNAI3,GNB2,MAP2K2,MAPK3	1.00E+00	NaN	CAMK2G,MAPK14,Ppp1r12a
Intrinsic Prothrombin Activation Pathway	9.55E-04	2	COL18A1,F9,FGA,FGG	2.14E-01	NaN	COL1A1,F13A1

Supplementary Table 5. Analysis of canonical pathways involved in basal vascular remodeling.

Shown are significant changes in the canonical pathways implicated in basal vascular remodeling, as defined by Ingenuity Pathway Analysis software, based on mass spectrometry analysis of tissue extracts from n=5 animals for each time point. Comparative p values and z-scores between baseline (no-ISO) and 2h post-ISO animals, and baseline and 7d post-ISO, respectively. Significantly over-represented terms (canonical pathways, functions, upstream regulators) were identified with a right-tailed Fisher's Exact Test that calculates an overlap p-value. The z-score was also calculated to assess the activation (positive z-score) or repression (negative one) of each term. The mass spectrometry proteomics data have been deposited to the ProteomeXchange Consortium via the PRIDE partner repository with the dataset identifier [PXD032667](https://www.ebi.ac.uk/pride/archive/study/PXD032667).

Canonical Pathways involved in basal tissue remodeling	2h vs. 0				7d vs. 0			
	p-value	z-score	Involved proteins		p-value	z-score	Involved proteins	
Cardiac β -adrenergic Signaling	4.58E-01	NaN	GNB2,PPP1R7		3.58E-01	-1	APEX1,ATP2A2,PPP1R7,PPP2R5D	
PI3K/AKT Signaling	4.79E-03	0.447	AKT2,ELP1,GSK3A,INPPL1,ITGA6,MAP2K2,MAPK3		1.00E+00	NaN	INPPL1,ITGA6,PPP2R5D,YWHAE	
mTOR Signaling	2.57E-02	NaN	AKT2,MAPK3,RPS16,RPS21,RPS6,RPS9		1.35E-02	NaN	EIF3A,EIF3B,EIF3C,EIF3I,EIF3M,EIF4B,EIF4G3,PPP2R5D,PRKAA2,RPS16	
p70S6K Signaling	3.39E-03	2.449	AGT,AKT2,GNAI3,MAP2K2,MAPK3,RPS6		1.00E+00	NaN	PPP2R5D,YWHAE	
Role of NFAT in Cardiac Hypertrophy	1.07E-02	0.447	AKT2,GNAI3,GNB2,HDAC2,MAP2K2,MAPK3,MAPK9		1.00E+00	NaN	CAMK2G,MAPK14	
Natural Killer Cell Signaling	4.57E-02	1.342	AKT2,COL18A1,HSPA1A/HSPA1B,MAP2K2,MAPK3		1.00E+00	NaN	COL1A1,HSPA1A/HSPA1B,MAPK14	
IL-6 Signaling	1.45E-02	1	AKT2,ELP1,MAP2K2,MAPK3,MAPK9		3.07E-01	1	A2M,COL1A1,HSPB3,MAPK14	
IL-8 Signaling	6.76E-03	1.342	AKT2,ELP1,GNAI3,GNB2,MAP2K2,MAPK3,MAPK9		#N/A	-	#N/A	
3-phosphoinositide Degradation	2.95E-02	0.447	ACP6,INPPL1,NUDT5,PPP1R7,PTPMT1		1.22E-01	0.816	EPHX2,INPPL1,NUDT5,PPP1R7,PPP2R5D,PRUNE1	
D-myo-inositol (1,4,5)-Trisphosphate Biosynthesis	#N/A	-	#N/A		#N/A	-	#N/A	
Production of Nitric Oxide and Reactive Oxygen Species in Macrophages	4.37E-03	0.816	AKT2,APOA1,APOM,ELP1,MAPK3,MAPK9,PPP1R7		5.66E-01	0	APOA1,MAPK14,PPP1R7,PPP2R5D	
Regulation of Actin-based Motility by Rho	1.00E+00	NaN	ITGA6		3.67E-01	NaN	ARPC3,ITGA6,PPP1R7	
Integrin Signaling	2.12E-01	2	AKT2,ITGA6,MAP2K2,MAPK3		4.95E-01	1	ACTN2,ARF3,ARPC3,ITGA6,PPP1R7	
Glutathione Redox Reactions I	#N/A	-	#N/A		1.48E-02	NaN	GPX3,GSTM1,GSTM2	
Apelin Cardiomyocyte Signaling Pathway	2.45E-02	1	AKT2,GNAI3,MAPK3,MAPK9		1.00E+00	NaN	ATP2A2,MAPK14	
Apelin Endothelial Signaling Pathway	9.77E-03	1.342	AKT2,GNAI3,MAP2K2,MAPK3,MAPK9		1.00E+00	NaN	PRKAA2	
Xenobiotic Metabolism General Signaling Pathway	5.62E-03	0.816	AKT2,CUL3,GCLC,MAP2K2,MAPK3,MAPK9		1.00E+00	NaN	GSTM1,GSTM2,MAPK14	
Xenobiotic Metabolism PXR Signaling Pathway	1.42E-01	-1	ALDH16A1,ALDH1A1,ALDH3A2,PPP1R7		1.00E-01	-1.134	ALDH1A1,CAMK2G,GSTM1,GSTM2,MAOB,PPM1A,PPP1R7	
Xenobiotic Metabolism CAR Signaling Pathway	5.01E-02	-2.236	ALDH16A1,ALDH1A1,ALDH3A2,MAP2K2,MAPK3		5.52E-01	-1	ALDH1A1,GSTM1,GSTM2,PPP2R5D	
Adrenomedullin signaling pathway	6.46E-03	0.378	AKT2,C3,CFH,GSK3A,MAP2K2,MAPK3,MAPK9		1.00E+00	NaN	MAPK14	

Supplementary Table 6. Analysis of canonical pathways involved in basal tissue remodeling.

Shown are significant changes in the canonical pathways implicated in basal tissue remodeling, as defined by Ingenuity Pathway Analysis software, based on mass spectrometry analysis of tissue extracts from n=5 animals for each time point. Comparative p values and z-scores between baseline (no-ISO) and 2h post-ISO animals, and baseline and 7d post-ISO, respectively. Significantly over-represented terms (canonical pathways, functions, upstream regulators) were identified with a right-tailed Fisher's Exact Test that calculates an overlap p-value. The z-score was also calculated to assess the activation (positive z-score) or repression (negative one) of each term. The mass spectrometry proteomics data have been deposited to the ProteomeXchange Consortium via the PRIDE partner repository with the dataset identifier [PXD032667](https://www.ebi.ac.uk/pride/archive/study/PXD032667).